



# Lanthanum aluminate (110) $3 \times 1$ surface reconstruction

D. Kienzle, P. Koirala, L.D. Marks\*

Department of Materials Science and Engineering, Northwestern University, Evanston, IL 60208, United States



## ARTICLE INFO

### Article history:

Received 3 July 2014

Accepted 16 November 2014

Available online 24 November 2014

### Keywords:

Oxide surfaces

Density functional calculations

Electron microscopy

## ABSTRACT

This paper describes a  $3 \times 1$  surface reconstruction on the LAO (110) surface and its atomic structure analyzed from experimental electron diffraction data coupled with X-ray photoelectron spectroscopy analysis and reinforced by density functional theory calculations. We construct the multidimensional convex hull for the system with excess  $\text{Al}_2\text{O}_3$  and in the presence of water. All the evidence points towards the reconstruction being very similar to the  $3 \times 1$  reconstruction on the  $\text{SrTiO}_3$  (110) surface with two hydrogen atoms added for valence neutrality.

© 2014 Elsevier B.V. All rights reserved.

## 1. Introduction

Lanthanum aluminate has recently become the subject of a rapidly expanding research area focused on the properties of oxide heterostructures, specifically  $\text{SrTiO}_3/\text{LaAlO}_3$  interfaces [1–5]. A 2D electron gas at the interface of these two insulating materials arises along with interesting properties such as superconductivity [1,6], metal to insulator transitions [5], and magnetism [3] making it of interest for potential applications in microelectronics. However, putting together any  $\text{SrTiO}_3$  and  $\text{LaAlO}_3$  surfaces will not necessarily exhibit conductivity [2]. The unique properties have been attributed to an electronic reconstruction which compensates for the valence discontinuity of the polar  $\text{LaAlO}_3$  (001) surface with non-polar  $\text{SrTiO}_3$  (001). This has now been expanded to include contributions from structural deformations [2] and oxygen defects [2]. The fact that the properties of the interface can vary widely due to differences in structure and/or chemistry of only a few atomic layers on either side of the interface illustrates the need for understanding and controlling the atomic structure at the interface to achieve a desired property. Metal oxide interface engineering is a challenge to the scientific community, but on the other hand presents a great opportunity to discover heterostructures with novel properties for electronic device applications.

Despite the growth in  $\text{LaAlO}_3/\text{SrTiO}_3$  interface research, little is known about  $\text{LaAlO}_3$  (LAO) surfaces; publications to date are qualitative or assume simple bulk terminations (e.g. [7–15]) and are either just theoretical or just experimental without a detailed comparison. One reconstruction has been solved for the (001) surface, a  $(\sqrt{5} \times \sqrt{5})R26.6^\circ$  [16] and a few others have been reported but not solved. The first reported characterization by Mortada et al. [13] of the LAO (110) surface, observed a  $c(4 \times 2)$  reconstruction formed after annealing at 900 °C in UHV and

observed high-step terraces with fine-step details attributed to small-width facets after annealing in air at 1500 °C for 10–20 h.

This paper describes a  $3 \times 1$  surface reconstruction on the LAO (110) surface and its atomic structure analyzed from experimental electron diffraction data coupled with X-ray photoelectron spectroscopy (XPS) analysis and reinforced by density functional theory (DFT) calculations. We construct the multidimensional convex hull for the system with excess  $\text{Al}_2\text{O}_3$  and in the presence of water. All the evidence points towards the reconstruction being very similar to the  $3 \times 1$  reconstruction on  $\text{SrTiO}_3$  (110) [17], with two hydrogen atoms added for valence neutrality.

## 2. Experimental

Self-supported single crystal TEM samples were prepared from LAO [110] single crystal substrates commercially purchased from MTI Corporation (Richmond, CA). The discs were mechanically thinned to thicknesses of  $\sim 100 \mu\text{m}$  with silicon carbide sandpaper, then dimpled with a Gatan 656 Dimple Grinder and 0.5  $\mu\text{m}$  diamond slurry until the thickness at the center was  $\sim 15 \mu\text{m}$ . The samples were then ion milled using a Gatan Precision Ion Polishing System with  $\text{Ar}^+$  ions at energies in the range of 3–4.5 keV for 1–3 h until a small hole could be seen with an optical microscope at 20 $\times$  magnification. A well-ordered  $3 \times 1$  surface was produced by annealing in air in a high-temperature tube furnace in the range of 1100–1200 °C for 5 h. Transmission electron microscopy (TEM) characterization of samples was done with a Hitachi H-8100 TEM operating at 200 kV. Bright field (BF) and dark field (DF) images as well as off-zone diffraction patterns were obtained. Diffraction patterns for the observed LAO (110)  $3 \times 1$  surface reconstruction were recorded using photographic film with exposure times ranging from 1 to 90 s and digitized using an Optronics P-1000 microdensitometer with a 25  $\mu\text{m}$  pixel size. Spot intensities arising from the  $3 \times 1$  surface were measured using a cross-correlation technique [18] and symmetry equivalent multiple measurements merged to create a single data set

\* Corresponding author.

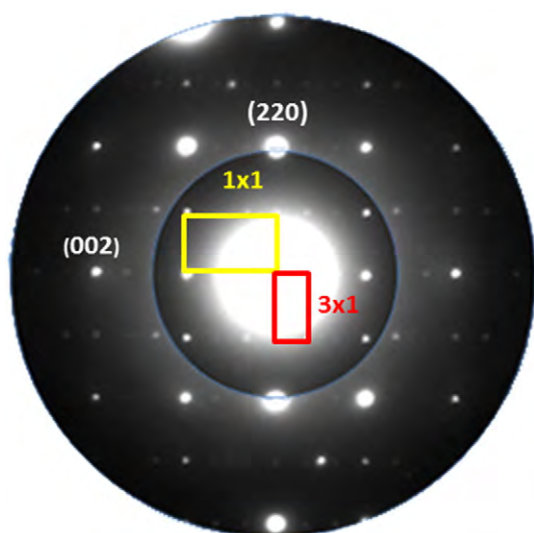


**Fig. 1.** Off-zone TED pattern of  $\text{LaAlO}_3$  (110) with a  $3 \times 1$  surface reconstruction. The  $1 \times 1$  surface cell is outlined in yellow with the  $3 \times 1$  cell in red.

of 51 independent beams for further analysis. The symmetry-independent diffraction data was analyzed by direct methods [19–22], which is automated into the edm [23] code. These analyses provide a series of plausible arrangements of the atoms at the surface that match the experimentally obtained diffraction intensities.

DFT was employed to determine the atomic positions in the out-of-plane direction perpendicular to the surface, as well as to check the agreement of in-plane atomic positions and calculate surface energies. In addition to the PBEsol [24] generalized gradient approximation the revTPSS method [25] was used and also an on-site exact-exchange parameter of 0.335 for the La-*d* band levels, chosen so that the rhombohedral LAO lattice parameter was correct to partially compensate for overbonding of the La-*d* levels with the O-*sp*, although the effect of this was minor; only results for the simpler PBEsol and revTPSS which is more accurate for the long-range contributions outside the surface are shown here. Muffin tin radii (RMT) of 2.36, 1.65, 1.25, and 0.5 bohr for La, Al, O, and H respectively were used. An RKMAX (product of smallest atomic sphere radius  $R_{\text{MT}}$  and the largest K-vector ( $K_{\text{max}}$ ))

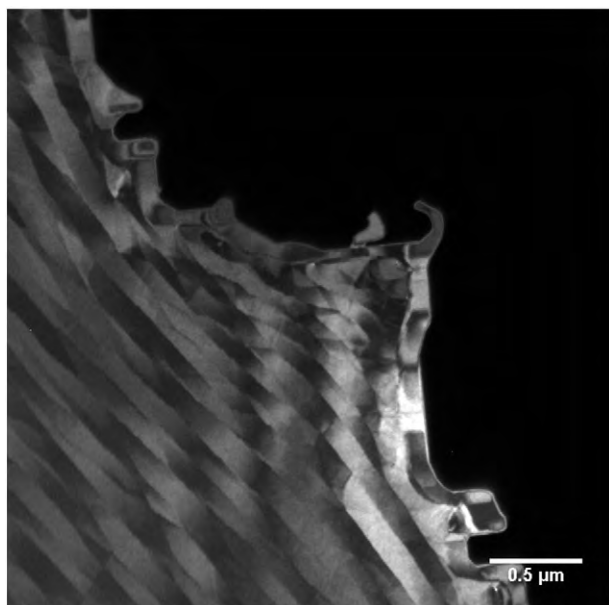


**Fig. 2.** DF TEM image of the  $3 \times 1$  reconstructed  $\text{LaAlO}_3$  (110) surface.

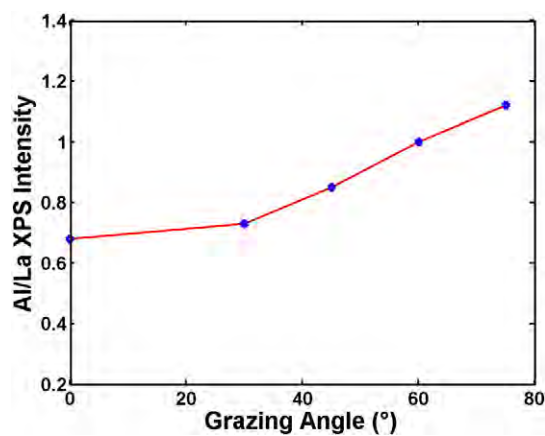


**Fig. 3.** Ratio of Al/La XPS intensity peak areas (La 4d, Al 2p) adjusted by relative sensitivity factors versus the angle between the surface normal and the detector. As the angle becomes more grazing, the effective surface sensitivity increases. Al concentration increases relative to La as fewer atomic surface layers are sampled.

cutoff of 5.85 and a *k*-mesh density corresponding to sampling 6-points along the  $\frac{1}{2}(110)$  direction in reciprocal space ( $\sim 0.3 \text{ nm}^{-1}$  between points) were used.

Surfaces were modeled as 3D periodic slabs starting from the in-plane positions from edm and DFT-optimized bulk lattice parameters with 8 layers of LAO bulk separated by  $\sim 10 \text{ \AA}$  of vacuum in the *z*-direction and infinitely extending in the *x*- and *y*-directions, e.g. a  $1.132 \times 0.534 \times 3.738 \text{ nm}$  cell for the  $3 \times 1$ . All atomic positions were

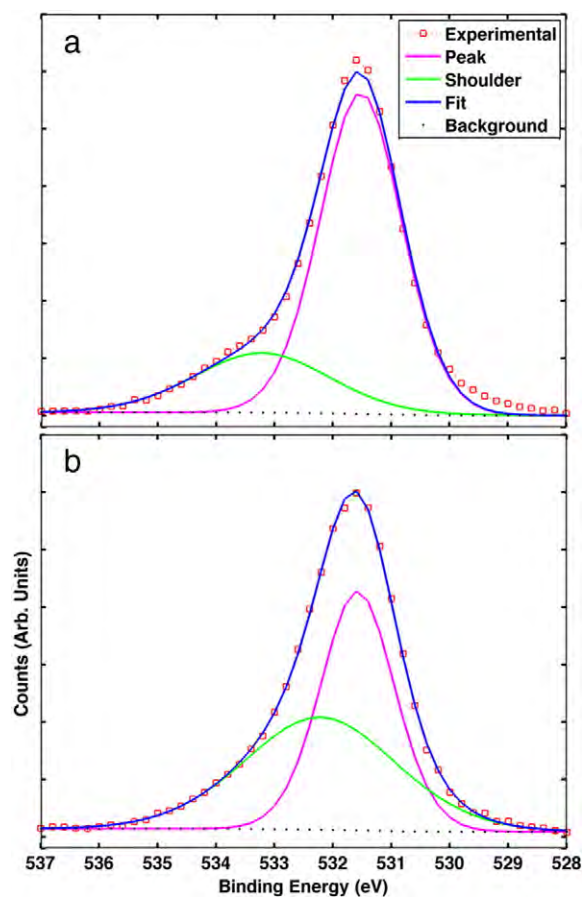


**Fig. 4.** XPS spectrum of the oxygen 1s peak (a) before annealing and (b) after annealing at  $650 \text{ }^\circ\text{C}$  for 3 h in  $1 \times 10^{-6}$  Torr  $\text{O}_2$  atmosphere.

relaxed to an accuracy of better than 0.01 eV per  $1 \times 1$  surface unit cell. The surface energy per  $1 \times 1$  surface unit cell ( $E_{\text{surf}}$ ) was calculated as  $E_{\text{surf}} = (E_{\text{slab}} - E_{\text{LAO}}N_{\text{LAO}} - E_{\text{AO}}N_{\text{AO}}) / (2N_{1 \times 1})$ , where  $E_{\text{slab}}$  is the total energy of the slab model,  $E_{\text{LAO}}$  and  $E_{\text{AO}}$  are the energies of bulk LAO and  $\text{Al}_2\text{O}_3$ , respectively,  $N_{\text{LAO}}$  and  $N_{\text{AO}}$  are the number of bulk LAO units and number of excess  $\text{Al}_2\text{O}_3$  units, respectively, and  $N_{1 \times 1}$  is the number of  $1 \times 1$  surface cells. Error bars of 0.05 eV/ $1 \times 1$  were assigned representing the average standard deviation between energies calculated using the PBEsol and revTPSS DFT functionals, after removing a global shift of the surface energies of about 0.4 eV/ $1 \times 1$  where revTPSS results are higher (as expected).

While DFT is a powerful technique, it is important to cross-check against known materials and for this Bond-Valence Sum (BVS) methods [26] can be powerful. These were calculated using *KDist* in the *Kalvados* program suite [27] including bonding contributions from up to 3.5 Å away with a *b* value of 0.37 used. Standard  $R_0$  values of 1.620 Å and 2.172 Å were used for  $\text{Al}^{3+} - \text{O}^{2-}$  and  $\text{La}^{3+} - \text{O}^{2-}$ , respectively [28]. For  $\text{H}^+ - \text{O}^{2-}$  bonds, a  $R_0$  of 0.957 Å corresponding to the O–H bond distance in gaseous  $\text{H}_2\text{O}$  was used [29]. Lattice parameters used for DFT calculations were renormalized to the experimental values by changing the volume isotropically prior to the BVS analysis; the adjustment was minor as PBEsol gave values very close to the correct bulk lattice parameters. Conventional BVS methods in the bulk are only accurate for octahedral  $\text{AlO}_6$  configurations, so we calculated the BVS for other oxides containing Al in a range of bonding configurations such as strontium aluminate ( $\text{SrAl}_4\text{O}_7$ ) [30]. This contains Al atoms that are bonded to 5 oxygen with an average BVS of 2.85 as well as Al bonded to 4 oxygen with a lower average BVS of 2.65. Another oxide, lanthanum hexaluminate [31], contains Al that can be 4, 5, and 6-fold coordinated with BVS values ranging from 2.43 (tetrahedral) to 2.97 (octahedral) which is closer to the BVS for Al in bulk LAO (2.85).

After TEM was used to confirm the presence of a LAO (110)  $3 \times 1$  reconstruction, sample was loaded into the SPEAR system [32] where XPS data was collected and the sample was also checked using the attached UHV-HREM operated at 300 kV. In this complex of chambers the base pressure of all chambers (including the microscope) is  $2 \times 10^{-10}$  Torr or better. A series of XPS spectra for the La 4d and Al 2p peaks were collected at varying angles of the sample surface normal relative to the detector to confirm the dominating surface species. Spectra for the O 1s peak were obtained before and after low temperature annealing in an attached gas cell to look for evidence of hydroxyl groups at the surface. We note that since the samples were annealed at temperatures 1100–1200 °C for 5 h to produce the reconstruction, low temperature annealing is exceedingly unlikely to change much except to drive off weakly chemisorbed species.

### 3. Results

An off-zone TEM diffraction pattern from a well-ordered  $3 \times 1$  surface (i.e. no streaking of spots) is shown in Fig. 1. The reconstruction was present in areas on the order of several microns squared and except for the  $3 \times 1$ , no other reconstructions were observed. A representative DF TEM image is shown in Fig. 2. The change of thickness is shown by clearly defined contrast changes showing that the surface has wide areas of flat terrace steps roughly 0.15 microns wide.

The ratio of peak areas for the Al peak and La peak at grazing angles of 0, 30, 45, 60, and 75° is plotted in Fig. 3. As the grazing angle of the surface normal with the detector increases, the effective sampling depth decreases making the technique more surface sensitive. Since the signal decreases as the grazing angle increases, it was difficult to get a signal past 75°. The ratio of Al to La increases with the grazing angle pointing to a surface with a higher concentration of Al than in the bulk. This indicates that the surface is Al-rich.

All XPS spectra reported here have been corrected for charging with reference to the adventitious 1s carbon peak. Further, the reported peak areas are a result of peak fitting using mixed Gaussian

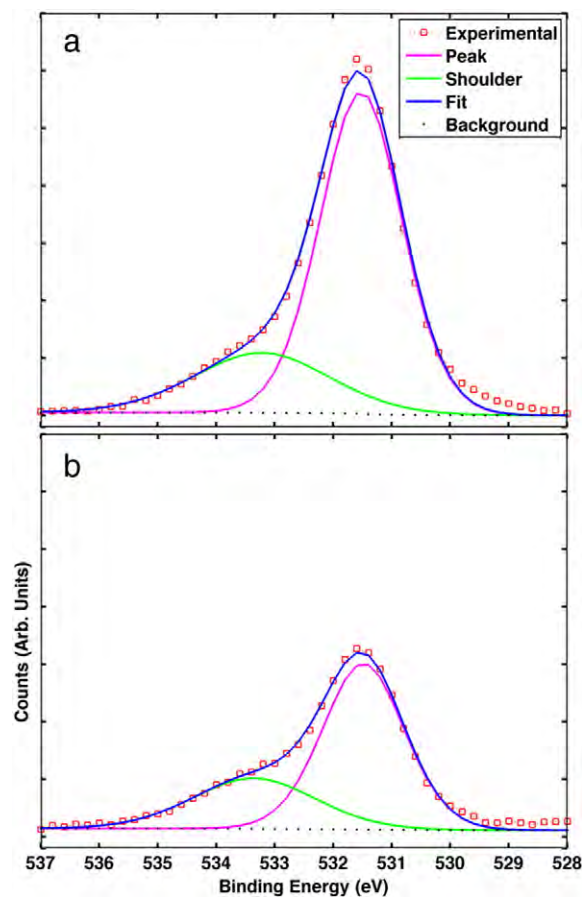


Fig. 5. XPS spectrum of the oxygen 1s peak at grazing angles of (a) 0° and (b) 45° to the surface normal.

and Lorentzian peak shapes. The fitting was performed with a convergence of  $1 \times 10^{-6}$  using a maximum of 20,000 iterations under the Powell algorithm [33].

XPS spectra of the O 1s peak are shown in Fig. 4. The  $3 \times 1$  reconstructed sample used for this scan was first identified with TED, baked overnight at  $\sim 200$  °C in a load-lock chamber, and introduced to the SPEAR UHV Analytical chamber for XPS. To determine if water plays a significant role in the structure formation i.e. is chemisorbed, XPS was done prior to and after annealing at 650 °C. This was done in a connected UHV chamber so that it could be filled with a low pressure of oxygen

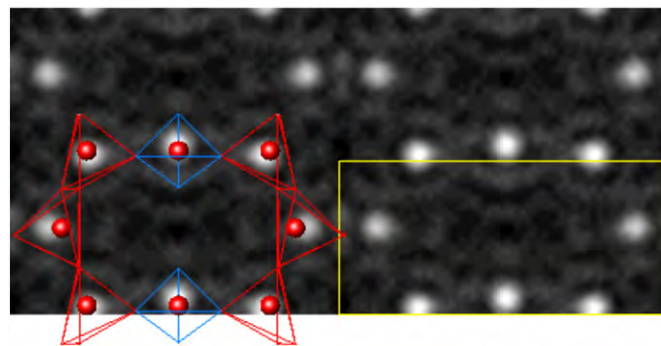


Fig. 6. EDM scattering potential map with surface unit cell outlined in yellow for  $\text{LaAlO}_3$  (110)  $3 \times 1$  surface reconstruction. To demonstrate the similarity to the  $\text{SrTiO}_3$  (110)  $3 \times 1$  reconstruction a cartoon of the structure is overlaid on the map showing six  $\text{TiO}_x$  polyhedra where red polyhedra represent  $\text{TiO}_5$  and blue represent  $\text{TiO}_4$ .

**Table 1**  
Table of LaAlO<sub>3</sub> (110) structures with DFT calculated surface energies.

Label	Cell	Description	Surface layer	Subsurface	Excess (AlO)	Excess (H <sub>2</sub> O)	Energy
B (2 × 1)	2 × 1	Bulk terminated layer with 2 oxygen vacancies	2O <sup>4-</sup>	2(O <sub>2</sub> <sup>4-</sup> )	0	-	1.95
F(3 × 1R_new2)	3 × 1	Surface network of rings of 6 AlO <sub>4</sub>	Al <sub>4</sub> O <sub>6</sub> <sup>6+</sup>	3(O <sub>2</sub> <sup>4-</sup> )	1.333	-	3.08
J(3 × 1AIR3)	3 × 1	F with additional AlO <sub>2</sub> in center of ring	Al <sub>6</sub> O <sub>6</sub> <sup>6+</sup>	3(O <sub>2</sub> <sup>4-</sup> )	2	-	3.91
M(N10a)	3 × 1	STO 3 × 1-type surface with Al <sub>5</sub> O <sub>5</sub>	Al <sub>10</sub> O <sub>12</sub> <sup>6+</sup>	3(O <sub>2</sub> <sup>4-</sup> )	3.333	-	3.91
P(N12)	3 × 1	STO 3 × 1-type surface with AlO <sub>2</sub> unit	Al <sub>6</sub> O <sub>8</sub>	3(Al <sub>2</sub> O <sub>2</sub> <sup>4+</sup> )	4	-	4.60
Wet-A(N8OH2)	3 × 1	STO 3 × 1-type surface with OH <sup>-</sup> unit on Al layer	Al <sub>5</sub> O <sub>7</sub> (OH)	3(Al <sub>2</sub> O <sub>2</sub> <sup>4+</sup> )	3.667	0.167	4.81
Wet-B(N12_rt5H)	3 × 1	STO 3 × 1-type surface with OH <sup>-</sup> unit on top bulk oxygen layer	Al <sub>5</sub> O <sub>4</sub> (OH) <sup>6+</sup>	3(O <sub>2</sub> <sup>4-</sup> )	1.667	0.167	3.26
Wet-C(N12Sat)	3 × 1	Similar to Wet-B saturated with OH <sup>-</sup> units	Al <sub>5</sub> O <sub>2</sub> (OH) <sub>5</sub> <sup>6+</sup>	3(O <sub>2</sub> <sup>4-</sup> )	1.667	0.833	1.55
Wet-D(1x1H)	1 × 1	Bulk terminated layer with two OH <sup>-</sup> units	(OH) <sub>2</sub> <sup>2-</sup>	LaAlO <sub>4</sub> <sup>+</sup>	0	2	0.44
Wet-E(1x1AH)	1 × 1	Al-rich 1 × 1 saturated with OH <sup>-</sup> units	(OH) <sub>2</sub> <sup>2-</sup>	Al <sub>2</sub> (OH) <sub>2</sub> <sup>4+</sup>	2	2	1.73

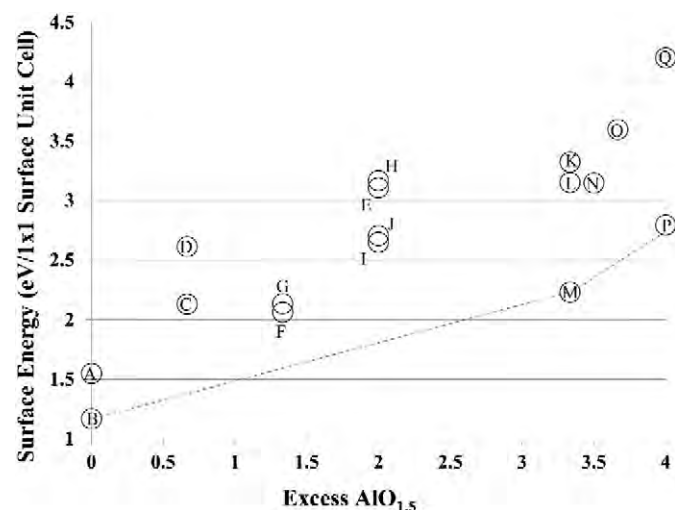
to avoid reducing the surface ( $1 \times 10^{-6}$  Torr). Note that annealing at 650 °C does not alter the surface structure as the reconstructions were observed only after annealing at high temperatures (1100–1200 °C).

Fig. 4(a) shows the main oxide peak in red with a maximum at 531.52 eV and a 1.69 eV higher binding energy shoulder at 533.21 eV. This is consistent with an O peak from aluminum oxide and a peak from surface hydroxyls separated by 1.6 eV, rather than a peak from O in molecularly adsorbed water which would result in a peak 3 eV higher in binding energy than the main oxide peak [34].

Before annealing, XPS spectra were recorded at 0° and 45° angles with respect to the surface normal as shown in Fig. 5. The ratio of the shoulder area to the peak area increased from 0.18 at 0° to 0.32 at 45° grazing angle indicating that the phenomenon causing the shoulder is located more towards the surface as expected for surface hydroxyls. After annealing, the curve fittings for the main peak and the shoulder have maximums separated by 0.7 eV compared to a 1.69 eV separation prior to annealing. Because of the separation in the post-anneal spectra, it is more likely that hydroxyl groups from the surface have been removed leaving an asymmetrical oxygen peak rather than a peak with hydroxyl shoulder. This data suggests that the surface could contain a small amount of chemisorbed water.

An estimate of the reconstructed surface composition and depth can be found using the Beer–Lambert equation for photoemission by a thin film:

$$I = I_0 \left[ 1 - \exp\left(-\frac{d}{\lambda \cos\theta}\right) \right]$$



**Fig. 7.** Plot of surface energies per  $1 \times 1$  bulk surface unit cell versus excess AlO<sub>1.5</sub> units at the surface. Convex hull is indicated by the dotted line connecting the lowest energy structures. Structures B, M, and P are described in Table 1; the rest are not described here further.

where,  $I$  is the intensity of electrons from a depth  $d$ ,  $I_0$  is the intensity of electrons from an infinitely thick sample, and  $\lambda$  is the attenuation length related to the inelastic mean free path of an electron in the sample. Comparing the intensity detected at the surface normal and at grazing angle ( $\theta$ ) results in the following:

$$d = -\lambda \cos\theta \left[ \ln\left(1 - \frac{I}{I_0}\right) \right]$$

To obtain an estimate of the depth of the Al rich surface reconstruction, a  $\lambda$  of 28.1 Å for an electron ejected from an Al atom with a binding energy of 74.6 eV [35] was used corresponding with the Al 2p peak energy. The normalized intensity ratio for the Al 2p peak area at 0° and  $\theta = 75^\circ$  is 0.19 ( $I/I_0$ ), resulting in a thickness of roughly 1.50 Å.

The edm analysis resulted in several scattering potential maps that were similar to or contained fragments of the solution as shown in

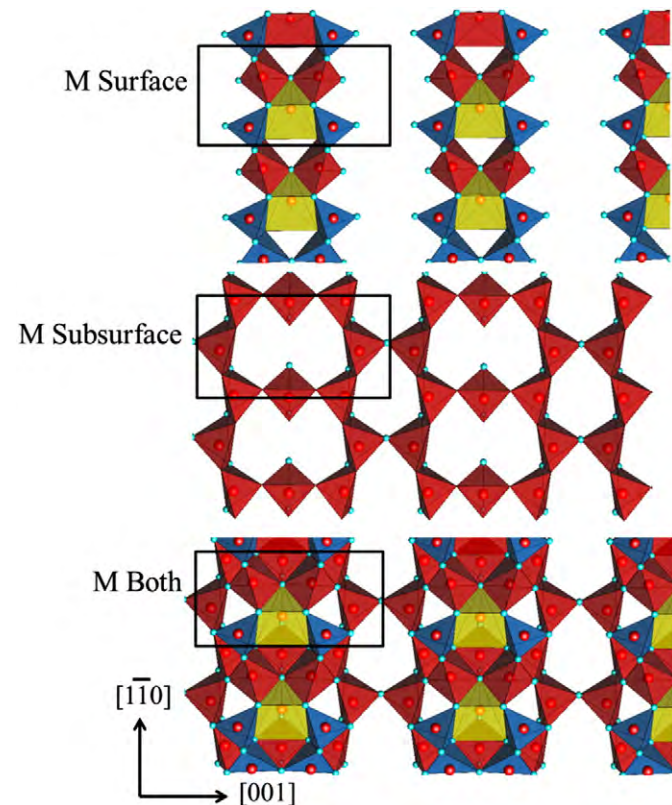


**Fig. 8.** Plan view of structure M's (N10a) surface consisting of the outermost surface layer (top) and the next layer below (middle) and a combined view of both layers together (bottom). The subsurface layer mimics the structure of the STO  $3 \times 1$  structure. Blue, red, and yellow polyhedra represent TiO<sub>4</sub>, TiO<sub>5</sub>, and TiO<sub>6</sub>, respectively.

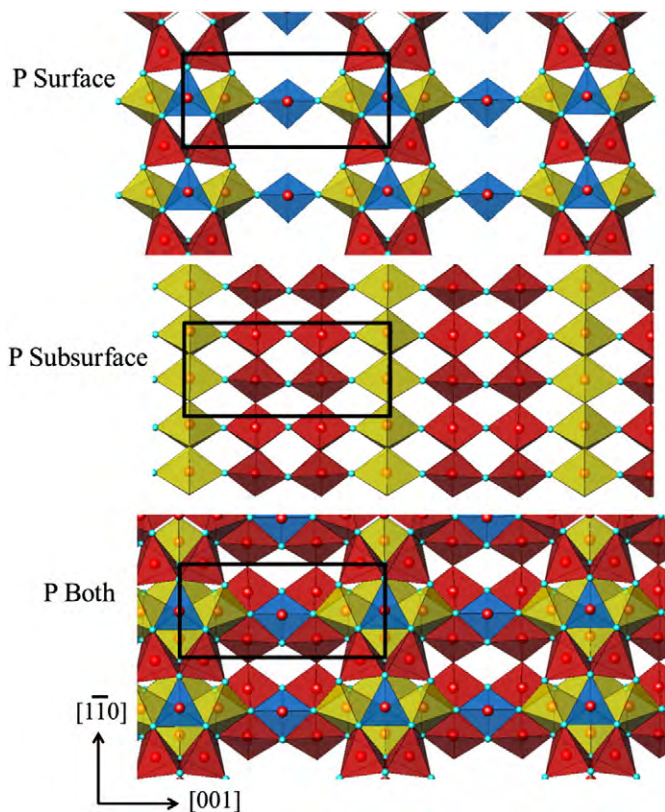


**Fig. 9.** Plan view of structure P's (N12) surface consisting of the outermost surface layer (top) and the next layer below (middle) and a combined view of both layers together (bottom). The surface layers mimics the STO  $3 \times 1$  structure with an additional  $\text{TiO}_4$  in the center of the smaller ring. Blue, red, and yellow polyhedra represent  $\text{TiO}_4$ ,  $\text{TiO}_5$ , and  $\text{TiO}_6$ , respectively.

**Fig. 6.** To probe which atoms were present at the bright spots in the map we compared refinement values for Al at those positions versus La. Aluminum and La gave similar  $R_f$  values, but the  $\chi^2$  for Al was significantly lower. This correlates with the results from XPS that show that the surface is Al-rich. The map looks very similar to those for the  $\text{SrTiO}_3$  (110)  $3 \times 1$

[17] and will be referred to STO  $3 \times 1$ . This point is illustrated by the high agreement of cation positions between the map and surface layer from the STO  $3 \times 1$  that is overlaid on the left. It refines very well with the experimental data having an  $R_f = 0.07$  and  $\chi^2 = 1.8$ .

However, the STO  $3 \times 1$  reconstruction cannot be directly used for LAO. The  $3 \times 1$  surface layer with  $x$ - and  $y$ -positions must fit onto a bulk layer and be valence neutral considering that it was prepared in oxygen. Along the [110] direction the bulk crystal structure of LAO consists of two alternating layers,  $\text{O}_2^{4-}$  and  $\text{LaAlO}_4^{4+}$  just as STO consists of  $\text{O}_2^{4-}$  and  $\text{SrTiO}_4^{4+}$  layers, but the difference in valence states of  $\text{Al}^{3+}$  and  $\text{Ti}^{4+}$  requires additional considerations for valence neutrality. The surface layer for STO contains 5 Ti and 7 O adding up to a valence state of  $5 \times 4 - 7 \times 2 = 6+$  which cancels with the  $6-$  from the bulk oxygen layer beneath it. LAO on the other hand would have a valence of  $5 \times 3 - 7 \times 2 = 1+$  and is not balanced. Since both aluminum and lanthanum are always  $3+$  valent in oxides, chemically unreasonable to use other valence states such as  $\text{Al}^{2+}$ ; these would be energetically extremely unfavorable.

Several ways were investigated to reach valence neutrality such as additional units to the STO-type  $3 \times 1$  and a similar network with 4 Al per surface unit cell arranged in 6-member polyhedra rings. Another way to reach valence neutrality is with hydroxyl groups and several structures incorporating  $\text{OH}^-$  were investigated as well. These structures are discussed further below. Two of the structures, M and P (refer to Table 1), which are variations on the STO  $3 \times 1$ -type structure and have low surface energies also refine reasonably well with  $R_f$  values of 0.10 and 0.15, respectively, although not as well as fitting with STO  $3 \times 1$  positions. Their  $\chi^2$  values, 3.5 and 3.9, respectively, are much higher most likely due to the greater number of atoms in the surface cell.

The wet surface structures Wet-A, Wet-B, and Wet-C have  $R_f$  values of 0.16, 0.20, and 0.20, respectively and  $\chi^2$  values of 1.9, 2.2, and 1.9, respectively. Overall the wet structures have slightly higher  $R_f$  values, but lower  $\chi^2$  values.

Part of the difficulty of using surface energies for this system is the lack of any previously solved comparison structures. As a frame of reference the stoichiometric  $\alpha\text{-Al}_2\text{O}_3$  (0001) and  $(1\bar{1}02)$  faces were calculated having surface energies of 2.9 and 2.3 eV respectively normalized to the LAO (110)  $1 \times 1$  surface cell.

A wide range of LAO (110) surface structures were optimized and their surface energies were calculated, as shown in Fig. 7. The details for a selected set of structures comprising those with the lowest calculated surface energies (B, M, P on the convex hull line and F and J near

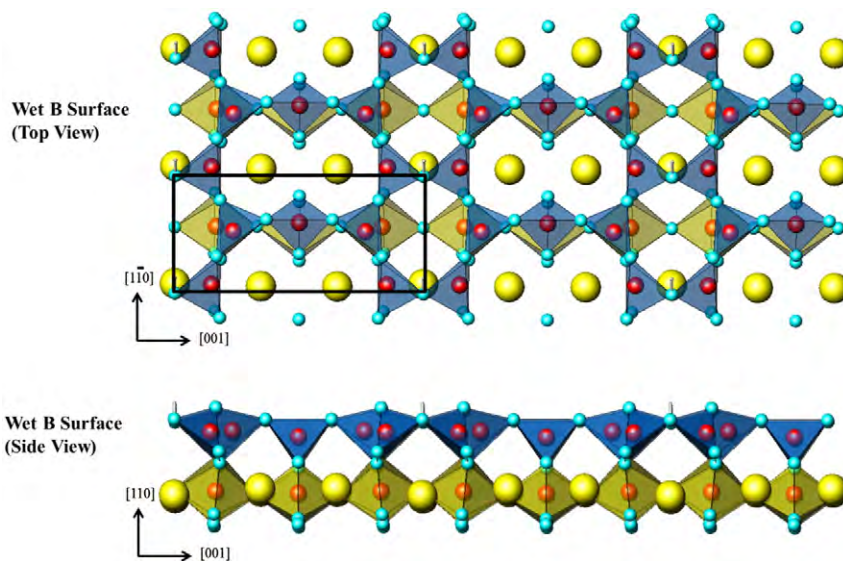


**Fig. 10.** Top view perpendicular to the Wet-B (N12\_rh5) structure surface and side view parallel to the surface. Blue and yellow polyhedra represent  $\text{TiO}_4$  and  $\text{TiO}_6$ , respectively. La, Al, O, and H atoms are in yellow, red, light blue and grey, respectively.

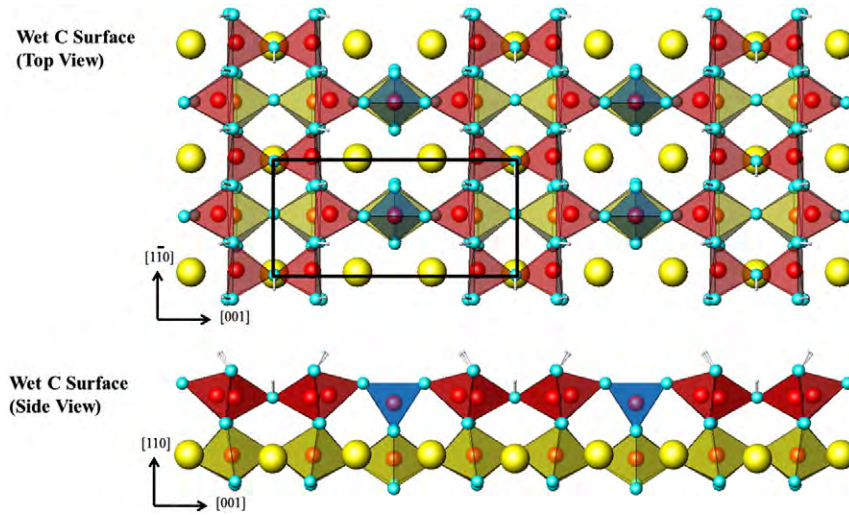


**Fig. 11.** Top view perpendicular to the Wet-C (N12Sat) structure surface and side view parallel to the surface. Blue, red and yellow polyhedra represent  $\text{TiO}_4$ ,  $\text{TiO}_5$ , and  $\text{TiO}_6$ , respectively. La, Al, O, and H atoms are in yellow, red, light blue and grey, respectively.

the line) are shown in Table 1 with their surface layer and subsurface layer composition, amount of excess  $\text{AlO}_{1.5}$  units, excess  $\text{H}_2\text{O}$ , and surface energy. The higher energy structures will not be discussed further here; details can be found in [36]. “Wet” structures were created based on the dry structures with the lowest surface energies and the  $\text{STO } 3 \times 1$  reconstruction.

Structure B is a simple LAO bulk terminated surfaces with two oxygen vacancies to balance the valance. Structure F is made up of a network structure of 6-member  $\text{AlO}_x$  polyhedra and J is a variation on F with a higher surface excess of Al resulting from an additional  $\text{AlO}_2$  in the center of one of the rings. This honeycomb network structure of  $\text{AlO}_x$  polyhedra is similar to that of  $\text{STO } 3 \times 1$  except that all of its rings are 6-member rings rather than alternating 6- and 8-member  $\text{TiO}_x$  rings. Structures M and P, however, are all based on the  $\text{STO } 3 \times 1$  network structure of alternating 6- and 8-member rings. Structure M, shown in Fig. 8 mimics the  $\text{STO } 3 \times 1$  surface layer as well as its subsurface layer of  $3(\text{O}_2^-)$ , but with an additional 5  $\text{AlO}_x$  polyhedra in the center of the larger ring at the outermost surface. Structure P shown in Fig. 9 has a higher excess of Al at the surface due to a bulk-like

subsurface layer of six  $\text{AlO}_x$  polyhedra and an additional  $\text{AlO}_2$  incorporated in the center of the smaller surface ring.

Additionally, several hydroxylated “wet” LAO surfaces were considered based on the  $\text{STO } 3 \times 1$  surface of alternating rings of 6 and 8  $\text{AlO}_x$  polyhedra, but with added  $\text{OH}^-$  to achieve valence neutrality. Wet-A has an  $\text{AlO}$  subsurface layer while Wet-B and Wet-C have a bulk oxygen subsurface layer. The difference between Wet-B and Wet-C is their surface water content; Wet-B has one additional  $\text{OH}^-$  per  $3 \times 1$  and Wet-C has 5 additional  $\text{OH}^-$  per  $3 \times 1$ . Two simple  $1 \times 1$  LAO structures, one with excess  $\text{H}_2\text{O}$  (Wet-D) and one with excess Al and  $\text{H}_2\text{O}$  (Wet-E), were included to aid in the comparison of the wet structures. Wet-B is shown in Fig. 10 and Wet-C is shown in Fig. 11.

The calculated surface energies are plotted in three-dimensions versus excess  $\text{AlO}_{1.5}$  and excess  $\text{H}_2\text{O}$  per  $1 \times 1$  surface in Fig. 12 and the overall surface energy range is reasonable compared to the alumina references. If we consider only the dry structures in the excess  $\text{AlO}_{1.5}$  vs. surface energy plane at zero excess  $\text{H}_2\text{O}$ , a convex hull line connects the lowest energy structures for each stoichiometry. Structure B, the bulk terminated layer with two O vacancies, M, and P define the convex

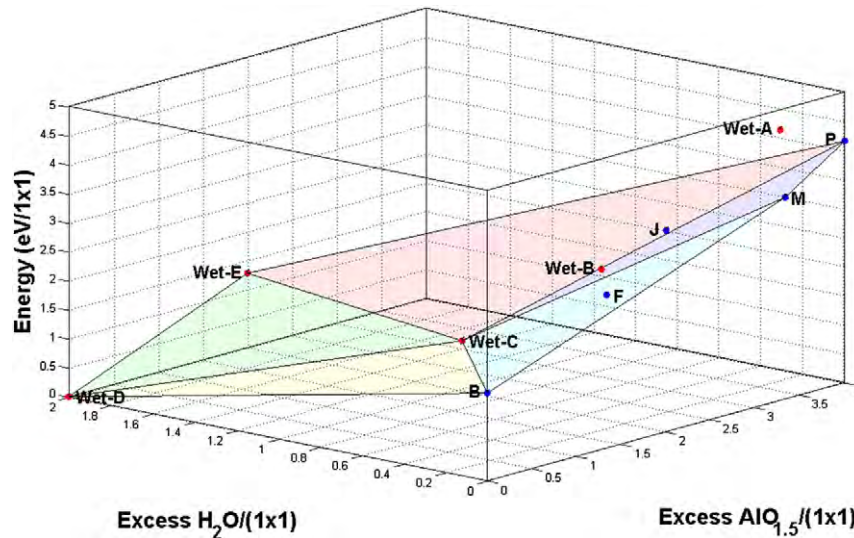


**Fig. 12.** Three-dimensional plot showing the calculated surface energy for  $\text{LaAlO}_3$  (110) surface structures relative to the amount of excess  $\text{AlO}_{1.5}$  on the x-axis and  $\text{H}_2\text{O}$  on the y-axis. Dry structure markers are blue and hydroxylated structure markers are red. Colored planes form the convex hull connecting the lowest energy structures. Surface energies are relative to the Wet-D energy.

**Table 2**  
Bond valence sums (BVS), coordination number (CN) and multiplicity within the cell (Mult.) for atoms in the surface and subsurface layer for structures B, M, and P. Average BVS are references with respect to bulk BVS of Al (2.85) and O (−1.96).

	Structure B				Structure M				Structure P			
	Atom	BVS	CN	Mult.	Atom	BVS	CN	Mult.	Atom	BVS	CN	Mult.
Surface layer	Al1	2.56	5	2	Al34	2.63	6	2	Al13	2.97	4	1
	La5	2.41	9	2	Al45	2.46	6	1	Al5	2.71	6	2
	O2	−1.74	5	2	Al37	2.77	6	2	Al6	2.72	6	2
	O1	−1.26	3	2	O3	−1.99	4	1	Al15	2.40	5	1
					O6	−1.92	3	2	O31	−1.62	3	2
					O2	−1.59	2	2	O32	−1.86	3	2
Subsurface layer									O34	−1.59	3	1
	Al5	2.91	6	2	Al33	2.81	6	2	O29	−2.15	4	2
	La3	3.14	12	2	Al38	2.81	6	1	O30	−2.16	5	1
	O5	−1.99	6	2	Al39	2.61	6	2	O33	−2.10	5	1
	O3	−2.00	6	2	O7	−2.04	5	1	Al4	2.55	5	2
	O4	−2.00	6	2	O5	−1.81	5	2	Al3	2.68	5	2
					O4	−1.75	3	2	Al11	3.08	6	1
					O1	−1.90	3	2	Al7	2.59	6	1
									O1	−1.68	5	2
									O2	−1.31	4	2
Average Surface Al	−0.29				−0.02			O15	−1.71	4	1	
Average Surface O	0.46				−0.04			O16	−1.57	3	1	
Average Subsurface Al	0.06				−0.12				−0.14			
Average Subsurface O	−0.04				0.13				0.06			
									−0.14			
									0.42			

hull line. Both M and P are structures based on the STO  $3 \times 1$  with alternating 6- and 8-member  $\text{AlO}_x$  polyhedra.

Looking to the center of the plot, all the convex hull planes meet at the Wet-C structure so it is the most stable structure in that stoichiometric range. This is not surprising since the Wet-C structure is essentially analogous to the STO  $3 \times 1$  with added hydrogen. Wet-C also lies in the excess Al range consistent with XPS results. At higher amounts of excess water (i.e. higher water chemical potentials), the  $1 \times 1$  Wet-D and Wet-E structures define the convex hull plane. Moving from a Wet-C surface to higher chemical potentials may create a surface mixture of Wet-C, Wet-D, and Wet-E although the  $1 \times 1$  surfaces would not be detectable by TED. Moving from Wet-C to less  $\text{H}_2\text{O}$ , the surface may dehydrate to the Wet-B structure which is essentially the same polyhedral structure, but with one  $\text{OH}^-$ . Wet-B is also close enough to the convex hull so a Wet-C structure obtained while annealing at high temperatures in a wet environment and then cooled to room temperature would not dehydrate completely and retain its atomic arrangement. Converting to one of the dry structures would involve atomic rearrangement that may be kinetically limited.

The BVS for the three structures defining the convex hull, B, M, and P, are shown in Table 2 and for the Wet-B and Wet-C in Table 3. It is important that the local bonding via BVS is comparable to what is found in the bulk oxide. The average BVS at the bottom of the tables are referenced to  $\text{LaAlO}_3$  bulk values of 2.85, −1.96, and 3.04 for Al, O, and La, respectively, to better illustrate the deviation. The surface BVS numbers do not differ substantially from those of the reference oxides, reinforcing the structures' feasibility. The overall BVS for the Wet-C structure are closer to bulk values than Wet-B because of the additional  $\text{OH}^-$  that help improve the Al and O coordination.

#### 4. Discussion

One of the challenges faced when attempting to solve a surface structure such as the LAO  $3 \times 1$  is knowing when it has truly been solved. While correlation between the refined positions from diffraction data and the DFT stable positions suggests that a solution is correct, alone this is not a complete proof. Other conditions need to be met:

1. There must be a correlation between the refined positions from diffraction data and the DFT stable positions.

2. There should not be unchemical distortions of the underlying bulk material.
3. It must fit other constraints from the preparation conditions; here it needs to be a valence-neutral insulator with a respectable band gap.
4. The energy has to be reasonable with the surface part of the convex-hull construction. However, this is only a relative measure referenced to some bulk chemical potential, here  $\text{Al}_2\text{O}_3$ .
5. The local bonding must be reasonable, this being an absolute (not a relative) condition.

Addressing condition (1), M and P have decent refinement values, although the STO  $3 \times 1$ -type surface and wet structures refine better.

**Table 3**  
Bond valence sums (BVS), coordination number (CN) and multiplicity within the cell (Mult.) for atoms in the surface and subsurface layer for Wet structures B and C. BVS are references with respect to bulk BVS of Al (2.85) and O (−1.96).

	Structure Wet-B				Structure Wet-C			
	Atom	BVS	CN	Mult.	Atom	BVS	CN	Mult.
Surface	Al3	2.55	4	2	Al2	2.82	5	2
	Al4	2.48	4	2	Al3	2.68	5	2
	Al5	2.71	4	1	Al4	2.72	4	1
	O2	−1.51	2	2	O2	−1.57	2	2
	O26	−1.64	2	2	O26	−1.93	3	2
	O27	−1.27	3	1	O28	−2.00	3	2
	O3	−1.81	4	2	O27	−2.27	4	1
	O4	−2.20	4	2	O3	−1.90	4	1
	O15	−1.89	5	2	O4	−1.98	4	1
	O16	−1.65	5	2	O15	−1.70	5	2
	H1	0.87	1	1	O16	−1.79	5	2
					H1	0.90	1	1
					H2	0.96	1	2
					H3	0.90	1	2
Subsurface	La3	3.27	12	1	La3	3.03	11	2
	La8	3.29	12	2	La6	3.14	12	1
	Al2	2.61	6	2	Al6	2.93	6	2
	Al7	2.91	6	1	Al1	2.62	6	2
	O1	−1.66	5	1	O1	−1.60	5	2
	O5	−1.91	5	2	O5	−1.96	5	2
	Average surface Al	−0.30				−0.11		
Average surface O	0.22				0.10			
Average subsurface Al	−0.14				−0.07			
Average subsurface O	0.13				0.18			

It should be noted that a R1 value of 0.07, i.e. a 7% error in the intensities is very low for a surface structure. It is hard to say if this disqualifies M and P from being a solution for higher amounts of  $\text{AlO}_{1.5}$  at zero chemical potential of water. Both structures satisfy conditions (2) and (3) as well. More likely, since the LAO  $3 \times 1$  reconstruction was annealed at high temperatures in the presence of water and a hydroxyl shoulder was observed on the oxygen peak with XPS, the Wet-C structure is formed and persists at room temperature with perhaps varying amounts of hydroxyls such as the Wet-B. The wet structures satisfy conditions (2) and (3) also.

In the absence of solved LAO (110) surface structure to compare surface energies with, a large amount of structures were computed to reveal the energy region the surface most likely occupies. Condition (4) is met since the Wet-C structure defines the convex-hull. The BVS of structures are acceptable given the wide range of bond valence states that Al in oxide compounds can exist in, thus satisfying condition (5). All the data indicates that the LAO (110)  $3 \times 1$  reconstruction is the Wet-C structure remarkably similar to the STO (110)  $3 \times 1$  reconstruction, but with water. This is not surprising since both lanthanum and aluminum are very electropositive elements, with  $\text{LaAlO}_3$  much more ionic than  $\text{SrTiO}_3$  and as a consequence having a much higher affinity for water.

It is appropriate to make a few comments about how the reconstruction forms, using knowledge from the STO surfaces [37,38] as well as the MgO and NiO (111) surfaces [39,40]. It is reasonable that the initial ion-beam preparation of  $\text{ABO}_3$  perovskites leads to a slightly A deficient surface with a slight B excess. The ion-beam will create a reactive surface which will chemisorb water. The annealing process is then a competition between dehydration and ordering, a combination of kinetic and thermodynamic factors. The  $3 \times 1$  structure described here is a very stable structure, so it will be hard to remove the last two hydrogen atoms (although not completely impossible).

The results indicate that Al atoms at the surface have fewer bonds than octahedrally bonded Al in the bulk which allows for the creation of a stable 2D network of  $\text{AlO}_x$  at the surface. The behavior of Al at the surface may be closely related to network formers in glasses as has been suggested for the STO (001) surface [41]. Al is known to act as a network former and occupy tetrahedral sites in many materials, most commonly in aluminosilicate glasses [42]. Studies on aluminosilicate glasses and gels have shown that  $\text{Al}^{3+}$  can replace  $\text{Si}^{4+}$  as the tetrahedral network former and may form amorphous networks with irregular cross-linking for charge compensation rather than forming 5-fold coordinated Al [43]. In this way, the LAO surface can be imagined as a sheet of networked  $\text{AlO}_x$  polyhedra that order into a ring motif at temperatures above 1100 °C, producing the  $3 \times 1$  reconstruction aided by water. Thinking of the surface as a pseudo-glass network of rings is something that could be extended to other perovskites and is demonstrated in the recently determined  $\text{SrTiO}_3$  surface reconstructions: (110)  $3 \times 1$  [17] and (001)  $(\sqrt{13} \times \sqrt{13})R33.7^\circ$  [41].

## Acknowledgments

LDM acknowledges funding by the DOE on Grant No. DE-FG02-01ER45945; DK and PK by the NSF on grant number DMR-0710643.

## Appendix A. Supplementary data

Supplementary data to this article can be found online at <http://dx.doi.org/10.1016/j.susc.2014.11.016>.

## References

- [1] A. Ohtomo, H.Y. Hwang, *Nature* 427 (2004) 423.
- [2] J.I. Maurice, C. Carrétéro, M.J. Casanove, K. Bouzehouane, S. Guayard, É. Larquet, J.p. Contour, *Phys. Status Solidi A* 203 (2006) 2209.
- [3] A. Brinkman, M. Huijben, M. Van Zalk, J. Huijben, U. Zeitler, J.C. Maan, W.G. Van der Wiel, G. Rijnders, D.H.A. Blank, H. Hilgenkamp, *Nat. Mater.* 6 (2007) 493.
- [4] A.D. Caviglia, S. Gariglio, N. Reyren, D. Jaccard, T. Schneider, M. Gabay, S. Thiel, G. Hammerl, J. Mannhart, J.M. Triscone, *Nature* 456 (2008) 624.
- [5] Ariando, et al., *Nat. Commun.* 2 (2011) 188.
- [6] N. Reyren, et al., *Science* 317 (2007) 1196.
- [7] Z.L. Wang, *Surf. Sci.* 360 (1996) 180.
- [8] P.A.W. van der Heide, J.W. Rabalais, *Chem. Phys. Lett.* 297 (1998) 350.
- [9] J. Yao, P.B. Merrill, S.S. Perry, D. Marton, J.W. Rabalais, *J. Chem. Phys.* 108 (1998) 1645.
- [10] D.W. Kim, D.H. Kim, B.S. Kang, T.W. Noh, D.R. Lee, K.B. Lee, *Appl. Phys. Lett.* 74 (1999) 2176.
- [11] H. Kawanowa, H. Ozawa, M. Ohtsuki, Y. Gotoh, R. Souda, *Surf. Sci.* 506 (2002) 87.
- [12] D.A. Schmidt, T. Ohta, Q. Yu, M.A. Olmstead, *J. Appl. Phys.* 99 (2006) 113521.
- [13] H. Mortada, M. Derivaz, D. Dentel, J.-L. Bischoff, *Thin Solid Films* 517 (2008) 441.
- [14] H. Seo, A.A. Demkov, *Phys. Rev. B* 84 (2011) 045440.
- [15] M.Q. Gu, J.L. Wang, X.S. Wu, G.P. Zhang, *J. Phys. Chem. C* 116 (2012) 24993.
- [16] C.H. Lanier, J.M. Rondinelli, B. Deng, R. Kilaas, K.R. Poeppelmeier, L.D. Marks, *Phys. Rev. Lett.* 98 (2007) 086102.
- [17] J.A. Enterkin, A.K. Subramanian, B.C. Russell, M.R. Castell, K.R. Poeppelmeier, L.D. Marks, *Nat. Mater.* 9 (2010) 245.
- [18] P. Xu, G. Jayaram, L.D. Marks, *Ultramicroscopy* 53 (1994) 15.
- [19] C.J. Gilmore, L.D. Marks, D. Grozea, C. Collazo, E. Landree, R.D. Twisten, *Surf. Sci.* 381 (1997) 77.
- [20] E. Landree, C. Collazo-Davila, L.D. Marks, *Acta Crystallogr. B Struct. Sci.* 53 (1997) 916.
- [21] L.D. Marks, R. Plass, D. Dorset, *Surf. Rev. Lett.* 4 (1997) 1.
- [22] L.D. Marks, E. Bengu, C. Collazo-Davila, D. Grozea, E. Landree, C. Leslie, W. Sinkler, *Surf. Rev. Lett.* 5 (1998) 1087.
- [23] R. Kilaas, L.D. Marks, C.S. Own, *Ultramicroscopy* 102 (2005) 233.
- [24] J.P. Perdew, A. Ruzsinszky, G.I. Csonka, O.A. Vydrov, G.E. Scuseria, L.A. Constantin, X. Zhou, K. Burke, *Phys. Rev. Lett.* 100 (2008) 136406.
- [25] J.P. Perdew, A. Ruzsinszky, G.I. Csonka, L.A. Constantin, J. Sun, *Phys. Rev. Lett.* 103 (2009) 026403.
- [26] J.A. Enterkin, A.E. Becerra-Toledo, K.R. Poeppelmeier, L.D. Marks, *Surf. Sci.* 606 (2012) 344.
- [27] K. Knížek, *Kowalvos—Software for Crystal Structure and Powder Diffraction*, 2012.
- [28] I.D. Brown, *Accumulated Table of Bond Valence Parameters*, [http://www.iucr.org/\\_data/assets/file/0018/59004/bvparam2011.cif](http://www.iucr.org/_data/assets/file/0018/59004/bvparam2011.cif) 2011.
- [29] J.A. Enterkin, A Chemical Approach to Understanding Oxide Surface Structure and Reactivity, 2010.
- [30] E. Boyko, L.G. Wisnyl, *Acta Crystallogr.* 11 (1958) 444.
- [31] N. Iyi, Z. Inoue, S. Takekawa, S. Kimura, *J. Solid State Chem.* 54 (1984) 70.
- [32] C. Collazo-Davila, E. Landree, D. Grozea, G. Jayaram, R. Plass, P.C. Stair, L.D. Marks, *J. Microsc. Soc. Am.* 1 (1995) 267.
- [33] M.J.D. Powell, *Comput. J.* 7 (1965) 303.
- [34] J.B. Miller, S.L. Bernasek, J. Schwartz, *Langmuir* 10 (1994) 2629.
- [35] S. Tanuma, C.J. Powell, D.R. Penn, *Surf. Interface Anal.* 43 (2011) 689.
- [36] D. Kienzle, *Surface Structures of the Metal-Oxide Materials Strontium Titanate and Lanthanum Aluminate* Evanston, Northwestern University, IL, 2013.
- [37] A.E. Becerra-Toledo, M.R. Castell, L.D. Marks, *Surf. Sci.* 606 (2012) 762.
- [38] A.E. Becerra-Toledo, J.A. Enterkin, D.M. Kienzle, L.D. Marks, *Surf. Sci.* 606 (2012) 791.
- [39] J. Ciston, A. Subramanian, L.D. Marks, *Phys. Rev. B* 79 (2009) 085421.
- [40] J. Ciston, A. Subramanian, D.M. Kienzle, L.D. Marks, *Surf. Sci.* 604 (2010) 155.
- [41] D.M. Kienzle, A.E. Becerra-Toledo, L.D. Marks, *Phys. Rev. Lett.* 106 (2011) 176102.
- [42] V.V. Petkov, S.J. Billinge, S.D. Shastri, B. Himmel, *Phys. Rev. Lett.* 85 (2000) 3436.
- [43] K.J.D. MacKenzie, T. Kemmitt, R.H. Meinhold, M. Schmucker, L. Mayer, *J. Eur. Ceram. Soc.* 20 (2000) 645.